A Modeling Approach for MVDC Grid Planning and Evaluation of the Design Parameters

1st Katharina Hetzenecker
Institute for Power Generation and Storage Systems
E.ON Energy Research Center, RWTH Aachen University
Aachen, Germany
katharina.hetzenecker@eonerc.rwth-aachen.de

2nd Tim Karsten
Institute for Power Generation and Storage Systems
E.ON Energy Research Center, RWTH Aachen University
Aachen, Germany
tim.karsten@eonerc.rwth-aachen.de

3rd Jan Mathé
Institute for Power Generation and Storage Systems
E.ON Energy Research Center, RWTH Aachen University
Aachen, Germany
jan.mathe@eonerc.rwth-aachen.de

4th Rik W. De Doncker
Institute for Power Generation and Storage Systems
E.ON Energy Research Center, RWTH Aachen University
Aachen, Germany
post_pgs@eonerc.rwth-aachen.de

***Abstract*—The paper presents a modeling approach for medium-voltage dc grid planning and applies it to an example grid connecting a data center, climatization facilities, photovoltaic generation, and electric vehicle charging. The approach assesses the system's efficiency and installed nominal power, and through application to the example grid, the impact of different design choices is demonstrated. The evaluation shows that silicon carbide semiconductor switches and operating active front ends with a power-flow control algorithm can improve system efficiency and decrease the required nominal power for component design.**

***Index Terms*—MVDC, grid planning, converter efficiency, power-flow control**

I. Introduction

The advantages of dc technology in the high-voltage transmission sector are well documented, and it has become a widely used technology for high-voltage power transmission systems. Furthermore, there has been a growing trend of implementing low voltage dc (LVDC) projects, with examples like the DC-Industrie project in Germany, which showcased an LVDC microgrid for industrial use, and LVDC infrastructure installations in public buildings and along highways in the Netherlands [16] [17]. In addition, the development of standards for LVDC grids is already being prepared [1] [2].
As medium-voltage dc (MVDC) grids can connect elements between different LVDC systems, they also come into focus. MVDC grid designs offer several degrees of freedom to develop reliable and cost-effective grid infrastructure. One prominent example is the voltage level.

While medium voltage ac (MVAC) systems are defined in a relatively wide voltage range and are usually operated as a 10, 20, or 30 kV grid to supply low voltage grids, no decision has been made yet, regarding voltage levels of MVDC grids. The modeling approach for MVDC grid planning presented in this paper allows for an informed decision about the different design aspects of an MVDC grid. The planning is followed by evaluating design choices for an exemplary grid regarding efficiency and installed nominal power, which are indicators for operational and investment costs. The grid planning comprises the connection to an MVAC grid and the coupling to underlying LVDC systems.

Section II describes the development of the grid design process and explains how the efficiency of the different grid components is modeled. Section III applies the procedure to an example grid design for an MVDC grid.

This work was supported by the project HYPERRIDE, funded by the European Union's Horizon 2020 Research and Innovation Programme, under Grant 957788.

II. MVDC Grid Design Process

The following presents the most important components and design parameters of the MVDC grid design process and the general procedure. Figure 1 illustrates the proposed grid topology and the various degrees of freedom for the MVDC grid design. The grid topology contains the connection points of the MVDC distribution grid to the surrounding MVAC grid, referred to as substations. It also includes the connection of the MVDC grid to the power-consuming or power-generating appliances operating on the low-voltage level. The generated outputs of this process contain the required component sizing regarding nominal power and system losses. The results can be translated into investment costs and operational costs.
The process takes an MVDC and an LVDC grid voltage value U_{MVDC}, U_{LVDC}, the desired grid configuration, and load profiles of the LVDC appliances to be connected via the MVDC grid, as input parameters.
First, for these input parameters, a suitable MV/LV dc-dc converter topology is selected for each MV/LV dc-dc interface. Then, the nominal power to be installed for each connection to the LVDC appliance is determined. The MV/LV conversion losses are calculated and added to the existing load profile, considering the partial load efficiency of the converters. The resulting load profiles for the medium-voltage grid serve as

K. Hetzenecker, T. Karsten, J. Mathé and R. W. De Doncker, ""A Modeling Approach for MVDC Grid Planning and Evaluation of the Design Parameters," 2023 IEEE PES Innovative Smart Grid Technologies Europe (ISGT EUROPE), Grenoble, France, 2023, pp. 1-5, doi:10.1109/ISGTEUROPE56780.2023.10407529.

input for the selection of the cable cross-section A_{cable}. After A_{cable} and other required cable parameters have been determined, the power-flow calculation is performed over the entire length of the given load profiles to calculate the total MVDC power transmission losses and the power loading of the substations supplying the MVDC grid. Hence, the peak loading of each substation equals the minimum nominal power to be installed. The substation consists of a 50 Hz transformer connected to an active or passive rectifier unit, as depicted in Fig. 1. Based on the simulated efficiency of the corresponding converter topology, the converter losses of the substation can be determined. The transformer losses are calculated using the peak efficiency values prescribed in [13] and the course of the efficiency curve from [12]. The main adjustable parameters in this design process are the voltages on the MV and the LV side, as well as the types of switches and switching frequencies of the converter topologies. Also, if active front-ends are assumed, the application of power-flow control can be investigated. Whether this leads to a more efficient substation operation or potential material savings in the design will be analyzed using an example grid in Section III.

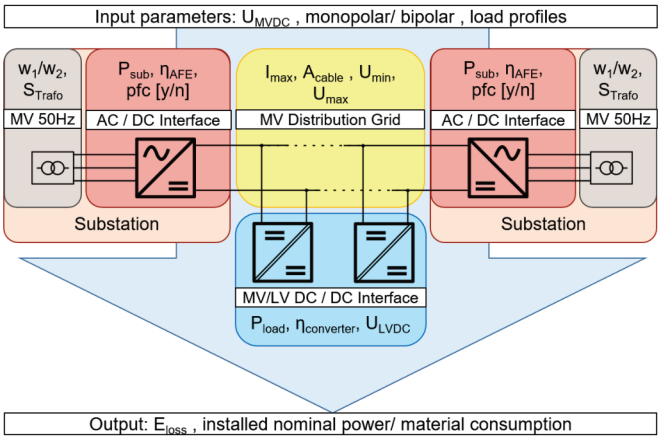

Fig. 1. Overview of design process for a MVDC grid that supplies LVDC appliances and is connected to the public MVAC grid.

A. Obtaining Converter Efficiency

The efficiency curves of the converters are obtained by simulation with PLECS® [4]. The information about switching losses, conduction losses, thermal resistance, and thermal capacity are taken from the manufacturer's datasheets. The temperature of the heatsink is assumed to be $T_{\mathrm{hs}} = 40\,^{\circ}\mathrm{C}$ and the simulated temperature in the switching modules never exceeded the rated maximum temperature $T_{\mathrm{lim}} = 120\,^{\circ}\mathrm{C}$.

B. MVDC-LVDC Converter Efficiency

A modular converter consisting of multiple three-phase dual-active bridges (DAB) in input-series output-parallel (ISOP) configuration is considered as connecting element between the medium and the low-voltage level. This topology offers flexibility and scalability, as it consists of identical modules and, at the same time, also benefits from the soft-switching operating mode the dual-active bridge is known for [8].

Several degrees of freedom exist for this converter design. Those correspond to the number of modules, which is directly related to the overall voltage on the MVDC side, as well as to the voltage on the primary side of each module U_{p}, the voltage on the secondary side U_{s}, the transformer winding ratio $\frac{n_1}{n_2}$, the switching frequency f_{sw}, the transformer's leakge inductance L_σ and the semiconductor technology of the switches. The impact of the nominal voltages on the primary and secondary side and the transformer winding ratio is summarized by the dynamic voltage ratio d, defined by (1). The dynamic voltage ratio influences the power transmission capability of the DAB, as shown in (2). Figure 2 depicts the module efficiency over the range of operation points up to the maximum module power for different combinations of values for U_{p} and U_{s}. To consider a symmetrical transformer design, the winding ratio is kept at $\frac{n_1}{n2} = 1$ for the scope of this paper. The leakage inductance of the transformer is assumed to be $L_\sigma = 64\,\mu\mathrm{H}$. For calculation of the efficiency models of the IGBT-module FF100R12KS4 and of the SiC Mosfets IMW120R007M1H from Infineon were used with a switching frequency of 10 kHz [10], [11]. It is assumed that the DAB designs allow maximum power transmission at $\varphi = \frac{\pi}{3}$ as for higher values of φ the reactive power consumption in the ac-link increases significantly [9]. In Fig. 2, the most power per module can be transferred with the DAB3 configuration In both cases, the efficiency over the different operation points is approximately constant because $d = 1$; thus, the DAB is operated in soft switching mode over the whole operation range. For the modules where U_{p} does not equal U_{s}, efficiency strongly declines in partial load operation, as $d = 0.6$ and the DAB operates under hard switching conditions. The SiC module has lower losses than the IGBT module, so the configuration DAB4 achieves the highest efficiency.

$$d = \frac{U_{\mathrm{s}}}{\frac{n_2}{n_1} U_{\mathrm{p}}} \tag{1}$$

$$P_{\mathrm{DAB}} = \frac{U_{\mathrm{p}}^2 d}{\omega L_\sigma}\left(\frac{2\varphi}{3} - \frac{\varphi^2}{2\pi}\right) \qquad \text{for } 0 \le \varphi \le \frac{\pi}{3} \tag{2}$$

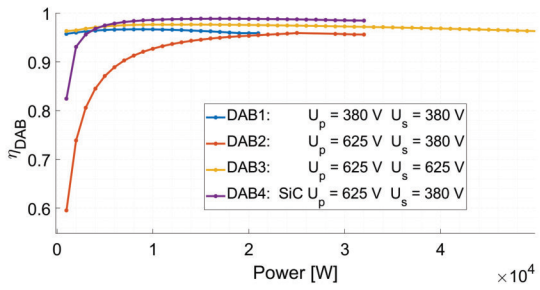

Fig. 2. Course of the DAB efficiency over different operating points, considering different voltage ratios of primary and secondary side, as well as different types of semiconductor switches.

K. Hetzenecker, T. Karsten, J. Mathé and R. W. De Doncker, ""A Modeling Approach for MVDC Grid Planning and Evaluation of the Design Parameters," 2023 IEEE PES Innovative Smart Grid Technologies Europe (ISGT EUROPE), Grenoble, France, 2023, pp. 1-5, doi:10.1109/ISGTEUROPE56780.2023.10407529.

C. Cable Cross Section

According to the given load profiles, the annual peak loading of the grid structure is determined. Afterward, a power-flow calculation based on MatACDC [6] is performed with generic cable parameters to calculate the maximum current $I_{\max}$. The suitable cable cross-section for $I_{\max}$ is subsequently determined according to the VDE norm 0276-620 [5]. Cable parameters corresponding to this cross-section are taken from [7] and are used in all following calculations. Next, the load-flow analysis is repeated to check if voltage band violations occur. If necessary, the cable cross-section is enhanced. For the calculations, a threshold margin of $\pm 10\%$ of U_{MVDC} was used, although in other cases, this value might be lower or higher depending on the local grid operator's demands.
Figure 3 shows the recommended current densities for aluminum cables, assuming a maximum conductor temperature of $90\,^{\circ}\mathrm{C}$ and a temperature of $20\,^{\circ}\mathrm{C}$ for the surrounding earth. The current density values in [5] are for three-phase ac systems, where all three conductors are usually more or less equally loaded. In contrast, bipolar dc systems consist of two approximately equally loaded conductors and a neutral conductor, which, assuming symmetrical loading, barely carries current. It is assumed that the recommended current density values can be used as a worst-case assessment to determine the cable cross-section.

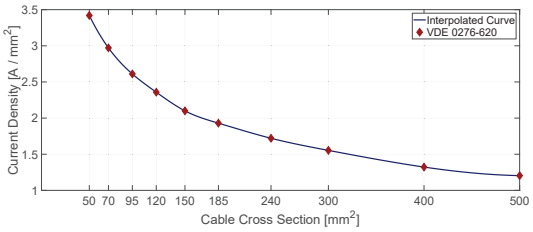

Fig. 3. Recommended cable cross sections for corresponding current densities in a triangular cable bundle considering thermal limits. [5]

D. MV AC/DC Converter Efficiency

Various converter topologies can connect the MVDC grid to the MVAC public ac grid. A passive topology, like a diode bridge converter, is more efficient than an active front end (AFE) as there are no switching losses. On the downside, the passive topologies cannot control the power they provide. Hence, in a dc grid supplied by more than one substation, the power loading of each substation depends on the distribution of loads in the grid and the connecting cables. This can necessitate a massive overdesign of substations if load centers are not evenly distributed among the grid area. In contrast, by deploying active topologies that allow for power-flow control, the design process can also consider the controllability and aim for a lower nominal power of the converters. Thus, in the following only AFEs are considered. Substations can balance their power loading using a three-level neutral point clamped converter (3L-NPC), and the pole-to-neutral voltages are evened out. Figure 4 depicts the efficiency for a 3-LNPC used for this analysis. In the simulation model used to obtain the efficiency curve, the ac-side voltage is $U_{\mathrm{AC}} = 3.3\,\mathrm{kV}$ and the dc-link voltage is $U_{\mathrm{DC}} = 5\,\mathrm{kV}$. The switching frequency is chosen as $f_{\mathrm{sw}} = 1\,\mathrm{kHz}$. The maximum efficiency is $\eta_{\max} = 98.5\%$ at a power $P = 0.1 P_{\mathrm{nom}}$.

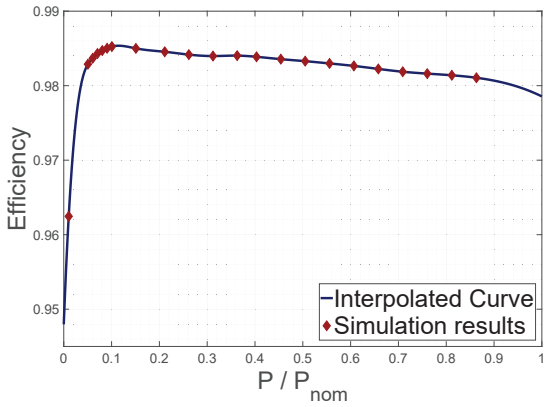

Fig. 4. Efficiency curve of the three level neutral-point-clamped converter over the range of operating points relative to nominal power.

E. Transformer Efficiency

Figure 5 shows the efficiencies of $50\,\mathrm{Hz}$ dry-type transformers with different nominal powers retrieved from [12], normalized to their respective maximum value. It can be seen that the efficiency profile for transformers of different rated powers is similar, and the operation point of maximum efficiency seems to always be at $P = 0.4 P_{\mathrm{nom}}$. As the curve of the $1000\,\mathrm{kVA}$ transformer is defined for the widest range of operation points from [12], this curve will serve as a base for the transformer efficiencies considered in this analysis. The efficiency curves are scaled to the efficiency values required by [13].

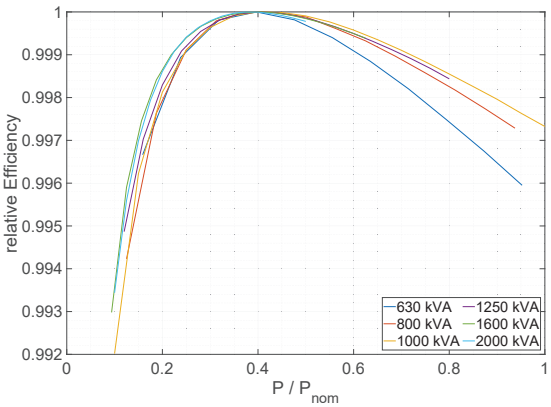

Fig. 5. Efficiency curves of $50\,\mathrm{Hz}$ transformers normalized to their maximum efficiency.

K. Hetzenecker, T. Karsten, J. Mathé and R. W. De Doncker, ""A Modeling Approach for MVDC Grid Planning and Evaluation of the Design Parameters," 2023 IEEE PES Innovative Smart Grid Technologies Europe (ISGT EUROPE), Grenoble, France, 2023, pp. 1-5, doi:10.1109/ISGTEUROPE56780.2023.10407529.

III. MVDC Grid Design Evaluation at the Example of a University Campus

This section applies the process described in the previous sections to an example grid design. At RWTH Aachen University, a new campus area will be built. This campus area includes a thermal network, a data center, PV power plants, and charging stations for electric vehicles. It is considered to connect these components using a customer-owned medium-voltage grid to maximize self-consumption. The load profiles modeling the power consumption and generation in hourly resolution over one year were developed in [14] and [15]. Based on the models, total annual energy demand sums up to $14.4\,\mathrm{GWh}$. A bipolar grid configuration was chosen, as they achieve higher efficiency, availability, and flexibility [3]. Figure 7 shows the load profiles of the data center, the energy center, and one example car park building. As all electrical equipment in the data center is assumed to operate 24/7, the load profile is at constant $1.6\,\mathrm{MW}$. The energy center supplies the area with heating and cooling, leading to a power consumption profile with seasonal variations that peak during summer. The load profiles of the car park buildings consist of the PV power plant generation on their rooftops and the power consumption of the charging stations in the building. Buildings P1-P4 have slightly different floor space sizes, resulting in different numbers of charging stations and different PV panel surfaces. However, the load profiles have similar characteristics as the solar radiation and the general utilization pattern of the charging stations is assumed to be the same. Further, it is assumed that the power generated by the PV power plants can be supplied directly to the charging stations. The load profile of each car park building is the residual power load, where negative power values describe power feed-in into the overlying MVDC grid and positive power values power demand. Since no applicable standardization for LVDC voltage levels exists, voltage levels promoted by the Current OS foundation of $350\,\mathrm{V}$ and $700\,\mathrm{V}$ for low voltage dc grids, with an upper boundary of the normal operation range of $380\,\mathrm{V}$ are considered [1]. Therefore, the LV voltage level is assumed to be $U_\mathrm{s} = \pm 380\,\mathrm{V}$. Figure 6 displays the general grid structure and illustrates the current flow within the grid for the maximum load according to the load profiles. The current values indicated by the color bar refer to the current per pole. For the analysis, it is assumed to have a grid voltage level of $U_\mathrm{MVDC} = \pm 2.5\,\mathrm{kV}$ in a bipolar grid configuration. The design process described in Section II is applied while varying the type of semiconductor switches used in the modular dc-dc converter and power flow control. In all three cases, the cable cross-section is calculated to $A_\mathrm{cable} = 300\,\mathrm{mm}^2$. Figure 8 depicts the accumulated annual losses for the different scenarios. The first bar shows the accumulated annual losses using the DAB2 configuration from Fig. 2 in the dc-dc converters. The resulting MV/LV dc-dc interface parameters are listed in Table II. Several converters are connected in parallel per interface to provide the necessary nominal power. The total annual loss energy sums up to

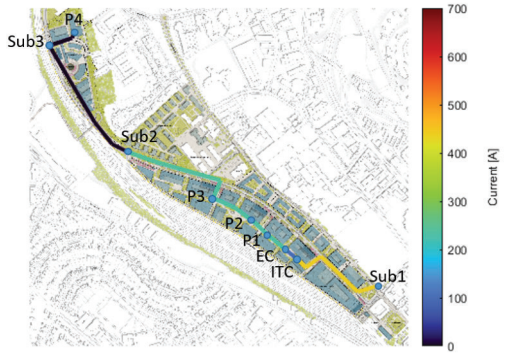

Fig. 6. Overview of the MVDC grid structure at Campus West including datacenter (ITC), an Energy Center (EC) with heatpumps and four car park buildings (P1-P4) containing EV charging stations and PV panels on the roof. Sub1-Sub3 represent the substations connecting the MVDC grid with the public MVAC grid. The maximum load power demand in the grid is $P_\mathrm{load,max} = 3.2\,\mathrm{MW}$, which results in a maximum current of $I_\mathrm{max} = 437\,\mathrm{A}$ per pole between Sub1 and the datacenter.

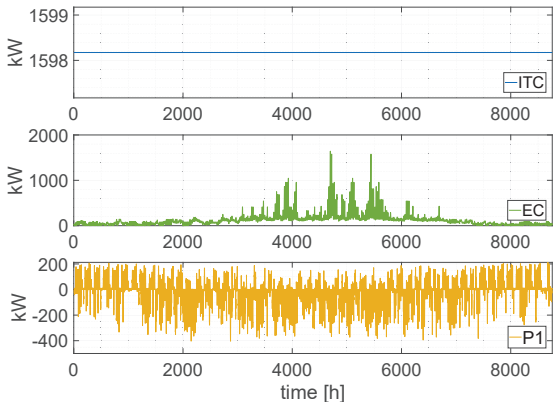

Fig. 7. Overview of example load profiles showing the power demand of the ITC, the EC and one car park building.

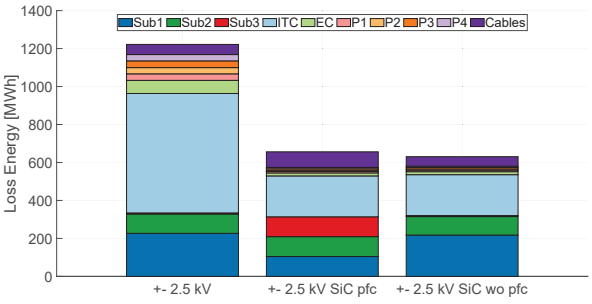

Fig. 8. Overview of annual losses and the impact of silicon carbide semiconductors, as well as the implementation of a power-flow-control algorithm on them.

K. Hetzenecker, T. Karsten, J. Mathé and R. W. De Doncker, ""A Modeling Approach for MVDC Grid Planning and Evaluation of the Design Parameters," 2023 IEEE PES Innovative Smart Grid Technologies Europe (ISGT EUROPE), Grenoble, France, 2023, pp. 1-5, doi:10.1109/ISGTEUROPE56780.2023.10407529.

$E_{\mathrm{loss,total}} = 1222\,\mathrm{MWh}$, of which with approximately $68\,\%$ is accounted for by the modular MV-LV dc-dc converters. This can be explained by the comparatively poor efficiency depicted in Fig. 2, especially in the partial load range. In particular, constantly supplying the data center is relevant here, as this causes ca. $75\,\%$ of the MV-LV conversion losses. As seen from the distribution of the substation losses, the power flow control is not applied here. Sub1 and Sub2 predominantly supply the power load of the grid, while Sub3, because of it's distance to the main loads, plays a minor role with $E_{\mathrm{loss,Sub3}} = 5\,\mathrm{MWh}$. The third bar depicts the same scenario but using the efficiency profile of the DAB4 configuration from Fig. 2. As expected with regards to the efficiency curve from Fig. 2, the overall losses were reduced to $E_{\mathrm{loss,total}} = 630\,\mathrm{MWh}$. Benefitting from the improved partial load efficiency, the converter losses of the car park buildings see the strongest relative reduction, with a decline to $21\,\%$ of its original value. While in absolute numbers, the converter losses in the data center declined the most. There, the original losses decline by $66\,\%$ from $629\,\mathrm{MWh}$ to $215\,\mathrm{MWh}$. When, in addition, a power-flow control is applied, the total losses incline by circa $26\,\mathrm{MWh}$, as the second bar in Fig. 8 shows. This can mainly be attributed to the increase in cable transmission losses. As the grid's power supply is now evenly distributed among the three substations, power is transmitted over longer distances, thus increasing the total losses. On the other hand, distributing the grid's power supply among all three substations allows for smaller component sizing, as seen from Table I. Additionally, the annual losses of all substations combined also decrease by about $7\,\mathrm{MWh}$.

TABLE I
NOMINAL POWER OF COMPONENTS IN SUBSTATIONS INSTALLED

Scenarios	**Sub1**	**Sub2**	**Sub3**
without pfc	2.5MW	1.6MW	1.6MW
with pfc	1.6MW	1.6MW	1.6MW

TABLE II
CONVERTERS INSTALLED IN MV/LV DC-DC INTERFACES

	ITC	**EC**	**P1**	**P2**	**P3**	**P4**
Converters per Interface	7	7	2	2	2	2
P_{nom} per converter	240 kW					
Modules per converter	8					

IV. SUMMARY AND CONCLUSION

This paper presents a modeling approach for assessing MVDC grid designs based on efficiency and installed nominal power, which can indicate material consumption and, thus, investment costs and CO_2 emissions. The approach is applied to an example case. The results show that the modeling approach allows for assessing the impact of design choices, like the type of semiconductor technology or the implementation of AFEs using a power-flow control algorithm. In the example case, implementing SiC semiconductor switches significantly increases the dc-dc converter efficiency. Operating the AFEs with a power-flow control that distributes the power loading equally among the substations allows for a decreased required nominal power for the component design. To further improve partial load efficiency, an adjustment of the winding ratio in the DAB transformers should be considered in future work.

REFERENCES

[1] Current OS Foundation, "Set of Rules - Voltages," https://currentos.foundation/ (accessed April 14, 2023).

[2] Emerge Alliance, " Standards," https://www.emergealliance.org/standards/our-standards/emerge-technical-standards-hierarchy/ (accessed April 14, 2023).

[3] S. Rivera, R. Lizana F., S. Kouro, T. Dragičević and B. Wu, "Bipolar DC Power Conversion: State-of-the-Art and Emerging Technologies," IEEE Journal of Emerging and Selected Topics in Power Electronics, vol. 9, no. 2, pp. 1192-1204, April 2021, doi: 10.1109/JESTPE.2020.2980994.

[4] "PLECS Manual," https://www.plexim.com/download/documentation (accessed April 14, 2023).

[5] VDE, DIN "VDE 0276-620: Starkstromkabel Energieverteilungskabel mit extrudierter Isolierung für Nennspannungen von 3,6/6 (7,2) kV bis einschließlich 20,8/36 (42) kV.," April 2018.

[6] J. Beerten , "MatACDC," . www.esat.kuleuven.be/electa/teaching/ matacdc/ University of Leuven (KU Leuven) Dept. Electrical Engineering (ESAT), Div. ELECTA Heverlee, Belgium, 2012.

[7] Südkabel,"Einadrige VPE-isolierte Kabel für Mittelspannungsnetze U_0/U 6/10kV – 18/30kV," https://suedkabel.de/downloads (accessed April 17,2023).

[8] R. W. A. A. De Doncker, D. M. Divan and M. H. Kheraluwala, "A three-phase soft-switched high-power-density DC/DC converter for high-power applications," in IEEE Transactions on Industry Applications, vol. 27, no. 1, pp. 63-73, Jan.-Feb. 1991, doi: 10.1109/28.67533 .

[9] R.Lenke, "A contribution to the design of isolated DC-DC converters for utility applications," Dissertation, RWTH Aachen, E.ON Energy Research Center, 2012.

[10] Infineon, "Technical Information FF100R12KS4," https://www.infineon.com/cms/de/product/power/igbt/igbt-modules/ff100r12ks4/ (accessed April 30, 2023)

[11] Infineon, "Technical information IMW120R007M1H," https://www.infineon.com/cms/de/product/power/mosfet/silicon-carbide/discretes/imw120r007m1h/ (accessed April 30, 2023)

[12] Siemens AG,"Technische Schriftreihe Ausgabe 16: Transformatorenauswahl in Abhängigkeit von Belastungsprofilen." 2016, https://assets.new.siemens.com/siemens/assets/api/uuid:d5c7ef0ed6ef6c74ce9a78ec9d6ad66a8da1f98d/ausgabe-16-transformatorauswahl-in-abhaengigkeit-von-belastungsp.pdf (accessed April 30, 2023)

[13] European Commission,"Commission regulation (EU) no 548/2014.", 2014, https://eur-lex.europa.eu/legal-content/DE/TXT/PDF/?uri=CELEX:32014R0548&from=EN (accessed April 30, 2023)

[14] Monti, A." Abschlussbericht zum Forschungsprojekt "Konzept für elektrische Energieversorgung in verschiedenen Ausbaustufen des Campus West der RWTH Aachen"."" 2020,Institute for Automation of Complex Power Systems E.ON Energy Research Center, RWTH Aachen.

[15] Müller, D." Zwischenbericht: Energiekonzept Campus West - Phase ii.",2020, RWTH Aachen University, E.ON Energieforschungszentrum Lehrstuhl für Gebäude und Raumklimatechnik.

[16] DC-Systems." Overview of completed and current projects." 2023, https://www.dc.systems/projects-2 (accessed April 30, 2023)

[17] ZVEI e.V."DC-INDUSTRIE", 2022, https://dc-industrie.zvei.org/ (accessed April 30, 2023)

K. Hetzenecker, T. Karsten, J. Mathé and R. W. De Doncker, ""A Modeling Approach for MVDC Grid Planning and Evaluation of the Design Parameters," 2023 IEEE PES Innovative Smart Grid Technologies Europe (ISGT EUROPE), Grenoble, France, 2023, pp. 1-5, doi:10.1109/ISGTEUROPE56780.2023.10407529.